Fluid jet access in topology optimization for cleanable parts

Giele, Reinier; Ayas, Can; Langelaar, Matthijs

DOI
10.1016/j.compstruc.2024.107420

Publication date
2024

Document Version
Final published version

Published in
Computers and Structures

Computers and Structures 301 (2024) 107420

Contents lists available at ScienceDirect

Computers and Structures

journal homepage: www.elsevier.com/locate/compstruc

Fluid jet access in topology optimization for cleanable parts

Reinier Giele *, Can Ayas, Matthijs Langelaar

Delft University of Technology, Mekelweg 2, 2628 CD, Delft, the Netherlands

ARTICLE INFO

Keywords:
Topology optimization
Cleanability
Jet access

ABSTRACT

Topology optimization methods are used to design high performance structural components that often have complex geometric layouts. In several industries, components are required to be cleanable, and for this research cleaning by jetting is considered. Thus, being able to ensure jet access on the entire surface of a structure is of interest in topology optimization. In this paper, a jetting filter is proposed, that turns a blueprint design into a jet accessible design. Two methods are considered to find an access field for each jet. These individual jet access fields are then combined into a total access field, to obtain a cleanable design. Consistent sensitivity analysis is used and the additional computational cost of the jetting filter is modest compared to the finite element analysis. The performance of the two methods is demonstrated with 2D and 3D numerical examples for mechanical and thermal topology optimization problems.

1. Introduction

Topology optimization (TO) is a computational design method for determining the geometric layout of a part for specific superior characteristics. Since TO does not rely on a specific initial design concept, it can systematically generate innovative geometric layouts, which could have been missed in the traditional design process. With increasing availability of TO techniques, their potential for industrial adoption also increases. In industry, often specific application requirements apply for the designs, for example manufacturability criteria. If manufacturing requirements are not considered during the TO, post-processing of the optimized design might be needed, which may counterweigh the gains achieved in performance by the TO. Consequently, in order to exploit the full potential of TO enabling wider industrial adoption, the relevant specific design requirements should be accounted for in the TO process.

In applications such as food processing, cleanroom equipment space, and medical instrumentation, it is often essential that components are *cleanable*. Cleaning can be performed through scrubbing and polishing, or through jetting a pressurized fluid. In this paper, the focus is on the latter given its prevalence in the mentioned industries.

In *jetting*, a pressurized cleaning agent such as air, water, or a cleaning liquid, is blasted towards the component, to remove contaminants from its surface. It is important that every surface that can be contaminated is completely cleanable. Assuming cleaning is only ensured through directly blasting the cleaning medium, i.e. ignoring reflected/redirected sprays, all surfaces should be directly accessible/reachable by a jet. In this paper, we assume the jet source to be a point source that can aim at any direction from a fixed position, although the presented method can also be adapted to jets with specific subsets of directions. The accessibility of a point on the component's surface depends on the overall geometric layout of the component. Thus, during TO it is essential to ensure cleanability by accounting for jet access as a design requirement. Integrating jet accessibility into TO would greatly improve the applicability of TO in numerous industrial applications.

To the best of our knowledge, no TO method considering jet accessibility currently exists. However, related research is available in the literature. Firstly, in the field of cleanability, Li et al. [13] presented a waterjet cleaning accessibility analysis. Campana et al. [6] quantified a component's cleanability using computational fluid dynamics. However, these studies do not involve TO. In our previous work, Giele et al. [9], cleanability is considered for TO, with the goal of ensuring drainability. However this did not involve jet accessibility requirements.

The more general topic of *accessibility* has been more widely studied in the field of TO. Chen et al. [7] developed a visibility map for TO and used it for ensuring manufacturability. This method considers for each element a visibility map on a sphere around the object, and compares this map to the visual capacity characteristics of manufacturing processes. This method's integration into TO however leads to a large number of constraints, and only cases where viewing directions align with structured mesh have been presented.

* Corresponding author.
E-mail address: r.j.p.giele@tudelft.nl (R. Giele).

https://doi.org/10.1016/j.compstruc.2024.107420
Received 7 September 2023; Accepted 19 May 2024
Available online 8 June 2024

Accessibility is also considered in relation to manufacturing constraints. In milling, except the case of slot milling, a straight line of access aligned with the tool orientation to the component's surface must exist. All material removed by the tool is then also accessible by a jet following the same trajectory, and thus, a millable part will also be cleanable when the corresponding jet positions and orientations can be chosen. TO filters for multi-axis milling are proposed by e.g. Langelaar [12], Mirzendehdel et al. [15] and Høghøj and Träff [11]. However, the tool translates with respect to the workpiece in milling, whereas in jetting, it is common to have jets mounted at a limited number of fixed positions, or a jet operator that can stand at certain positions relative to the part to be cleaned. From these fixed positions, a continuous range of jet orientations can be realized. The component's surface in Fig. 1a would be entirely accessible with multi-axis milling, while this is not the case with jetting from the four indicated jet positions. Therefore, jet accessibility cannot be represented by existing milling filters and requires a separate consideration.

For casting and molding the component is constrained to be created inside molds, which are later disassembled. So called undercut void regions prevent direct release and require the use of inserts, increasing complexity and cost. Thus, all mould space should be directly accessible in the parting direction. TO filters for casting and molding are for example presented respectively by Gersborg and Andreasen [8] and by Yoon and Ha [21]. However, similar to milling filters, the parting paths for the voids are parallel to each other, while in jetting the access is considered from a point source, and these existing methods therefore can not be applied for jet accessibility purposes.

In this study, a density based topology optimization method ensuring jet access for predefined jet positions is presented. The method is formulated as a filter, which ensures an input blueprint design to become jet-accessible. First, for each jet, an access field is created by the novel filter. We present and compare two methods for this step, one based on trajectory lines and another based on front propagation. Multiple access fields, one from each jet, are then combined into a total access field for all jets. Finally, this total access field is turned into a cleanable design with density field values in the range [0, 1]. As the entire surface area is accessible by at least one jet, the final design will not have internal voids. Therefore, next to the filter, a suggestion is given on how to apply the filter merely as an outer enclosure, in which internal holes are allowed. Two extra steps are introduced in the TO process to improve convergence and stability of the optimization process. The jetting constraint is activated gradually, and numerical stability is promoted by using the unfiltered design in the mechanical/thermal analysis and the filtered design in the volume determination. All steps needed for the proposed jetting filter are differentiable, allowing for gradient-based optimization.

This paper is organised as follows. In Section 2, the method is presented. Section 3 gives the numerical examples in 2D for with both ways of formulating the jet access filter, so that their performances can be compared. Next, for the approach with the most potential, 3D numerical examples are presented. The discussion and conclusions are given in Section 4 and 5, respectively.

2. Method

In this section, the jet access filter is presented. For clarity it is explained in 2D, subsequently its extension to 3D is given. Section 2.1 presents the general procedure and the overall structure of the filter. The individual steps of the filter are detailed in the subsequent subsections. Two different methods are presented to obtain a field that determines access for a single jet in Sections 2.2 and 2.3. Next, in Section 2.4 combining the access fields of multiple jets is discussed. In Section 2.5, how to obtain an accessible density field as output is shown. Section 2.6 focuses on the sensitivity analysis. Finally, in Section 2.7 a suggestion is given on how to use the filter to create an optimized jettable enclosure, so that internal holes are allowed to remain in the optimized structure.

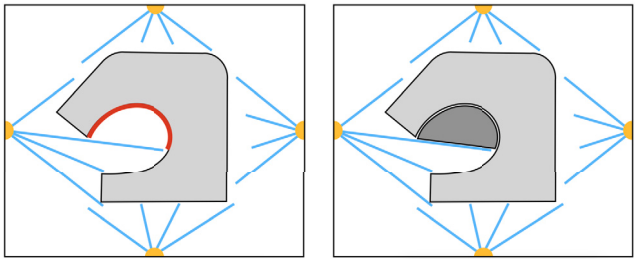

Fig. 1. Schematic illustration of the jet accessibility concept. Inaccessible surfaces are not allowed, thus inaccessible void area should be turned into solid. The structure is represented with light grey, the jets and jetting fluids are represented by the orange and blue, respectively. In (a) the inaccessible surface is marked in red, in (b) the inaccessible region is turned into solid represented by dark grey.

2.1. General procedure

Our aim is to have a filter for density based TO, on a structured grid, that produces jettable designs. We assume the jets have fixed positions and can blast in any direction. A jettable design entails the entire outer surface of the structure to be accessible from at least one jet. *Access* implies all points comprising the outer surface can be reached with a straight line emanating from at least one of the jets, without passing through any part of the structure.

Our jetting filter converts a blueprint design field $\mathbf{x}$ into a jettable design $\check{\mathbf{x}}$. This concept is schematically illustrated in Fig. 1. Contaminants can adhere at inaccessible parts of the surface, which can be prevented by filling of inaccessible void regions. The filter consists of several consecutive simple steps, where each step is a differentiable operation so that the sensitivities can be calculated easily with the chain rule. The whole procedure is illustrated in Fig. 2. Each step of this procedure is an independent operation, so other implementations with similar functionality can replace the ones presented in this paper.

The first step is smoothing of the blueprint design, using the convolution filter $\mathcal{F}$ from Bruns and Tortorelli [5] and Bourdin [3]. This is a standard step in density-based topology optimization to impose a length scale and prevent checkerboarding, and is not further explained. It is defined here as:

$$\tilde{\mathbf{x}} = \mathcal{F}(\mathbf{x}). \tag{1}$$

In the second step, an access field ${}^{j}\hat{x}$ is generated for each jet j. A point in the domain is accessible as long as no solid appears in a straight line connecting the point of interest and the jet source. This can be checked by emanating straight lines from the jet source into the domain, and keeping track of the element density values encountered along the way. The principle to convert any design into a valid jettable design, is that in the filtered design, an element further downstream (away from the jet) can not have a density lower than the elements encountered earlier. Two methods are proposed for executing this step, explained in Sections 2.2 and 2.3. Both methods have advantages and disadvantages in theory and implementation. The results are compared in Section 3.

The third step is to combine the access fields of individual jets into a total access field $\hat{x}$. In this step, if a point is accessible by at least one jet, it is considered accessible. Note that the values in the access fields ${}^{j}\hat{x}$ and $\hat{x}$ are not ensured to be in the range [0, 1]. This step is elaborated in Section 2.4. The fourth step is to turn the total access field into a density field $\check{x}$. The transformation step for intermediate accessible elements can be done strictly, or more approximately. This is discussed in Section 2.5.

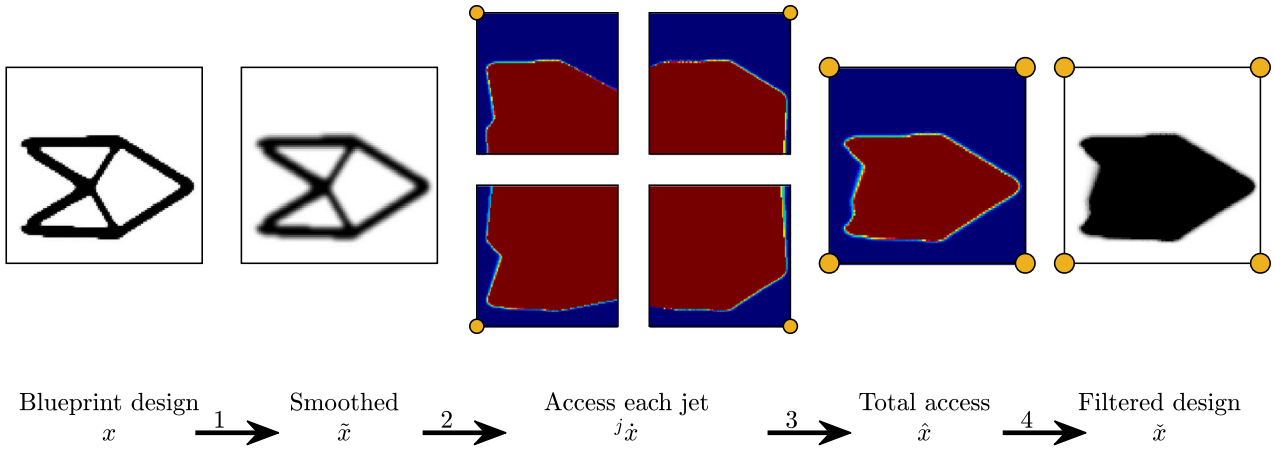

Fig. 2. Procedure from blueprint design x to cleanable design $\check{x}$. To illustrate the process 4 jets are used, positioned in the outer corners. The steps are indicated by the arrows. The values in the individual and total access fields ${}^{j}\dot{x}$ and $\hat{x}$ are not ensured to be in the range [0, 1] and are therefore represented in another color scheme.

2.2. Jet trajectory method

The first method to obtain an access field for a single jet is denoted the jet trajectory method. This method is inspired by part of the milling filter presented by Langelaar [12]. The goal is to check the accessibility of all locations in the domain for a jet, by analyzing the smoothed blueprint densities that are encountered on the way from the jet source to the location of interest. In this method, trajectory lines are defined from the source into the domain, along which the total density is calculated between selected points on the line and the jet source. This procedure consists of 3 substeps: i) determine the trajectory lines emanating from a jet and its representation on a structured grid, ii) determine the accessibility along each line, iii) combine the information of multiple lines for the same element.

In the first substep, the origin of each line, i.e. the jet location, is connected to the centers of all elements comprising the domain boundaries. Each trajectory line is then represented by a set of elements on the discretized domain that form an approximate representation of the line. For this purpose, the Bresenham line algorithm [4] is used, for simplicity. For a line l, the starting point position vector $\mathbf{L}_a^l$ and the end point position vector $\mathbf{L}_b^l$ are both assumed to be located in the center of an element for simplicity. The position of $\mathbf{L}_b^l$ with respect to $\mathbf{L}_a^l$ is $\Delta\mathbf{L}^l = \mathbf{L}_b^l - \mathbf{L}_a^l$, which determines the slope of the line. Bresenham defines multiple octants of line slope orientations, and for lines with $|\Delta L_x^l| > |\Delta L_y^l|$ one element is selected in every column, for lines with $|\Delta L_y^l| > |\Delta L_x^l|$ one element is selected in every row. Here, ΔL_x^l and ΔL_y^l are the x and y components of the vector $\Delta\mathbf{L}^l$. This is illustrated in Fig. 3. Consider the line aiming at the right boundary in Fig. 3b, where the elements that best describe the line are highlighted by pink. These were selected by choosing one element from every column, of which the element centre is closest to the line. With simple geometric rules, the element center within each column that is closest to a line is determined. The set of elements which are selected for jet j and line l in downstream order, is referred to as ${}^{j}A^{l}$, and the total number of elements in the set is ${}^{j}n^{l}$.

In the second substep, the accessibility along each line is calculated, computing the cumulative sum of element densities on each trajectory line from start to end. Similar to the multi-axis milling filter by Langelaar [12] the cumulative sum is preferred over a series of smooth maximum operations, as the former adds less nonlinearity for the optimization. This however implies that access field values can exceed 1. This substep is illustrated in Fig. 4 and can be written as:

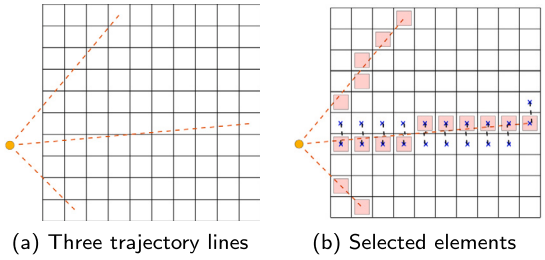

Fig. 3. Trajectory lines are used to check accessibility. In (a) three example lines are shown with each an origin point and an end point. In (b) it is shown that the closest elements along the trajectory line are used to form an approximation of the line on the discretized grid. The pink squares indicate the elements that are selected to describe each line, the blue points around the line aiming at the right boundary show how the distance from an element center to the line can be calculated.

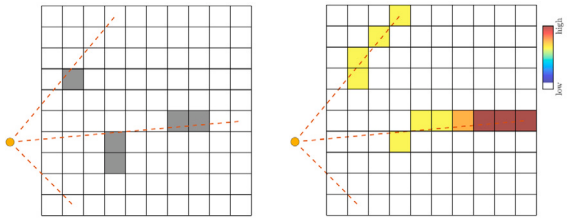

Fig. 4. The accessibility along three trajectory lines is measured, by cumulative summation of the encountered densities.

$$
\begin{aligned}
{}^{j}\ddot{x}_{\alpha}^{l} &= {}^{j}\tilde{x}_{\alpha}^{l}, && \text{for } \alpha = {}^{j}A_1^l,\\
{}^{j}\ddot{x}_{\alpha}^{l} &= {}^{j}\ddot{x}_{\beta}^{l} + {}^{j}\tilde{x}_{\alpha}^{l}, && \text{with } \alpha = {}^{j}A_i^l \text{ and } \beta = {}^{j}A_{i-1}^l,\\
& && \text{for } 2 \le i \le {}^{j}n^{l},
\end{aligned}
\tag{2}
$$

in which $\tilde{x}$ is the input element density which is taken for all elements in ${}^{j}A^{l}$ up till element α, and ${}^{j}\ddot{x}_{\alpha}^{l}$ is the element summation value for line l in element α.

In the third substep, multiple lines going through the same element have to be handled consistently. Especially in the vicinity of the jet, many lines go through the same elements. It is necessary to define an unambiguous elemental access value for this situation. In this work, the average is taken, for simplicity and linearity:

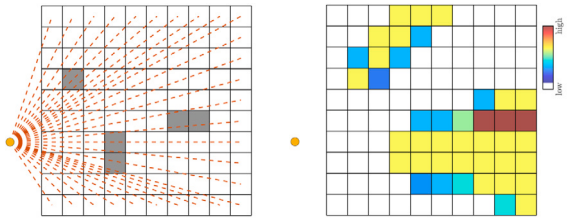

(a) Original density field (b) Access field

Fig. 5. Graphical representation of all trajectory lines covering all elements. The accessibility along all trajectory lines is combined by averaging cumulative densities in elements contained in multiple lines. The average cumulative density values can be much higher than 1.

$$ {}^{j}\dot{x}_e = \frac{\sum_{l=1}^{\ddot{n}_e} {}^{j}\ddot{x}_e^{l}}{\ddot{n}_e}, \tag{3} $$

where ${}^{j}\ddot{x}_e^{l}$ is the contribution in element e of line l, and $\ddot{n}_e$ are the total number of line contributions for this element. The result can be seen in Fig. 5.

The advantage of the presented jet trajectory approach is its simplicity. The outcome is a directionally summed density field, which is a measure for accessibility, as unobstructed trajectories maintain a zero value. Its extension to 3D requires no adjustments apart from accounting for the third dimension in the trajectory mapping procedure. Also a parallel computation is possible, either by handling parts of the trajectory line by separate processors and later add summation values of upstream parts in the line, or by processing different lines on different processors. However, since the operation is cheap, sequential calculation is not computationally costly.

2.3. Front propagation method

The second method to obtain an access field is through front propagation. This method is inspired by the additive manufacturing filter presented in van de Ven et al. [19], where anisotropic front propagation is used to distinguish supported and unsupported regions of a part upon addition of layers during additive manufacturing. Here, the goal is to check the accessibility of all locations in the domain, by analyzing the smoothed blueprint densities that are encountered on the way from the jet source to the location of interest. In this method, this is done by propagating a front from the jetting source into the design domain, and calculating the arrival time field. The propagation speed is isotropic but is reduced linearly with the local element density $\tilde{x}$. The time delay compared to an unobstructed reference time field then indicates accessibility. This procedure consists of 3 substeps: i) calculate the reference arrival time field, ii) calculate the density-dependent arrival time field, iii) compute the delay caused by the density field as a measure of accessibility. An example of this approach can be seen in Fig. 6.

In the first substep, the front propagation arrival time field T_1 is calculated, which is independent of the density field. This field will serve as a reference, to determine the delay caused by the densities. Front propagation with an isotropic speed function is used, which is given by:

$$ |\nabla T_1| F = 1, \tag{4} $$

where T_1 is the resulting arrival time function, F is the propagation speed, an initial time $T_1 = 0$ is set at the jet location. In our implementation, the Fast Marching Method is used, presented in Sethian [16].

In the second substep, the front propagation arrival time field T_2 is calculated, which depends on the filtered blueprint densities $\tilde{x}$. The front propagation equation now includes that the front moves slower through solid elements than through void elements:

$$ |\nabla T_2| F(\tilde{x}) = 1. \tag{5} $$

The slowdown is based on the local density value, and on a lower bound for speed parameter to prevent infinite arrival times. The speed through an element F_e is calculated with:

$$ F_e(\tilde{x}_e) = F_{\min} + \left(1 - \tilde{x}_e\right)\left(1 - F_{\min}\right), \tag{6} $$

where $F_{\min} < 1$ is the minimum speed parameter, and $\tilde{x}_e$ is the element density.

In the third substep, the delay field $\tau(\mathbf{x})$ is obtained. This field serves as the measure of accessibility. The delay is simply calculated by subtracting the first arrival time field T_1 from the second arrival time field $T_2(\mathbf{x})$, and is directly used as access field $\dot{x}$:

$$ {}^{j}\dot{x}(\tilde{x}) = \tau(\tilde{x}) = T_2(\tilde{x}) - T_1. \tag{7} $$

Any point for which the time delay $\dot{x} > 0$ cannot be reached by the jet in a straight line, see Fig. 6d.

A potential advantage of the presented approach is in the wake that is visible in the delay field. The gradient in the delay field could provide useful information to the optimizer regarding the proximity of an accessible region. The downside of the approach is that the front propagation on a discrete grid shows a discretization effect, which can result in delays also in areas outside the direct wake of the solid area (see also Fig. 6e). Also, an extra parameter $F_{\min}$ is introduced. The effect of this $F_{\min}$ parameter is visualized in Fig. 6f, which was created using a smaller $F_{\min}$ than used for the other figures. This can lead to an increase in the delay in and behind solid regions.

For jet locations outside the domain, one has to use initial arrival times on the boundary surfaces nearest to the jet position, which can be computed simply by Euclidian distance. The computational effort of this method is usually comparable to the jet trajectory method. An extension to 3D is trivial. For a parallel implementation, the reader is referred to e.g. Herrmann [10] or Yang and Stern [20].

2.4. Combining multiple jets

By now the access field ${}^{j}\dot{\mathbf{x}}$ can be calculated for each jet separately, either as a directional cumulative density field or as a time delay field. Next, these access fields for the separate jets have to be combined into one total access field, $\hat{\mathbf{x}}$. Here the lowest access value is relevant for each element, since a single jet access is sufficient for cleanability. This can be obtained in a differentiable manner by applying the P-norm smooth minimum operator over the access fields of the different jets:

$$ \hat{x}_e(x) = \left(\sum_{j=1}^{N} ({}^{j}\dot{x}_e)^{P_1} \right)^{\frac{1}{P_1}}. \tag{8} $$

Here, $P_1 < 0$ is the aggregation parameter, and N is the number of jets. The total access fields for a simple density distribution and two jets can be seen in Fig. 7.

2.5. Design output

Finally, the total access field has to be converted to a density field. The access field can have values on the order of the maximum number of elements in all directions. This has to be converted back to the density range of [0, 1]. Several functions can be used for this projection. In this work a P-norm minimum function is used, involving the total access field and the maximum density value of 1:

$$ \check{x}_e(x) = \left(1 + \hat{x}_e^{P_2}\right)^{\frac{1}{P_2}}. \tag{9} $$

Again, P_2 is the aggregation parameter which is a negative value. The resulting relation between the accessibility values and the density values is shown in Fig. 8.

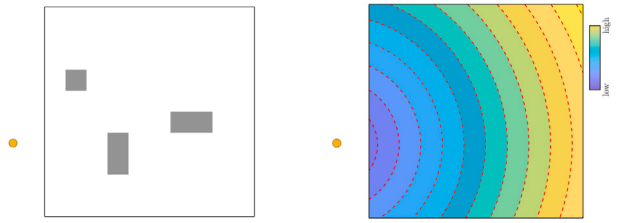

(a) Original density field

(b) Arrival time field independent of density

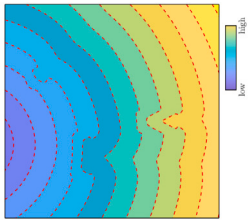

(c) Arrival time field dependent on density

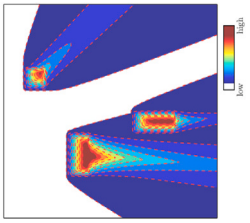

(d) Arrival time delay field

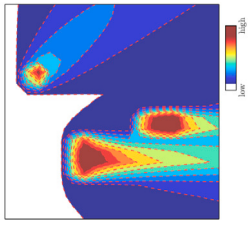

(e) Arrival time delay field, on a 20×20 element mesh

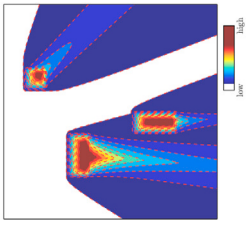

(f) Arrival time delay field, with $F_{\min} = 0.0001$

Fig. 6. Graphical representation of the front propagation approach. For a clear visualization these figures, except (e), have been obtained on a 100×100 element mesh. Figures (c), (d), and (e), were created with $F_{\min} = 0.1$.

2.6. Sensitivity analysis

Most of the steps in the filter procedure have straightforward sensitivity operations, such as the density filter in Step 1, and the P-norms in Step 3 and 4. This section will focus on the sensitivities of Step 2 only for the jet trajectory method. For the sensitivity analysis of the front propagation method, the reader is referred to van de Ven et al. [19].
For this an elementwise sensitivity ${}^{j}\dot{s}_e$ for a general function g is assumed, so that ${}^{j}\dot{s}_e = \frac{\partial g}{\partial {}^{j}\dot{x}_e}$. For the jet trajectory method, by going back the steps taken in Section 2.2 the input sensitivities are first divided by the number of line contributions for $\ddot{n}_e$:

$$ {}^{j}\ddot{s}_e = \frac{{}^{j}\dot{s}_e}{\ddot{n}_e}. \tag{10} $$

Next, the cumulative sum of element sensitivities on each trajectory line ${}^{j}\dot{s}_i^l$ is computed from the end of line to the start of the line:

$$ \begin{aligned} {}^{j}\dot{s}_\alpha^l &= \ddot{s}_\alpha^l, && \text{with } \alpha = {}^{j}A_i^l, \quad \text{for } i = {}^{j}n^l \\ {}^{j}\dot{s}_\alpha^l &= {}^{j}\dot{s}_\beta^l + \ddot{s}_\alpha^l, && \text{with } \alpha = {}^{j}A_i^l \text{ and } \beta = {}^{j}A_{i+1}^l, \quad \text{for } 1 \le i \le {}^{j}n^l - 1. \end{aligned} \tag{11} $$

The final output sensitivities $\tilde{\mathbf{s}}$ are obtained by summing up the contributions of all lines and all jets:

$$ \tilde{s}_e = \sum_{j=1}^{N} \sum_{l=1}^{\ddot{n}_e} {}^{j}\dot{s}_e^l. \tag{12} $$

2.7. Jettable enclosure

The jetting method introduced above does not allow output density fields with internal voids, as these cannot be accessed from outside. This may be overly restrictive for some applications. In this section, a modification is suggested to allow internal voids in a structure with a jettable outer enclosure. This jettable enclosure is part of the TO problem and is load-bearing, and within the enclosure internal voids are allowed. Since this is not the focus of the paper, only a short description is given here.

To obtain a jettable enclosure, the jetting filter can be combined with existing methods for creating a coating. The full procedure is shown in Fig. 9. The first steps are the same as in Fig. 2. Step 1: a smoothed design is created, with a density filter. Step 2: a jettable design with values in the range [0, 1] is obtained. Step 3: the jettable design field is transformed into an enclosure, using the erosion-based interface identification method from Luo et al. [14]. That is, after applying a second density filter to create intermediate density boundaries, and applying two Heaviside projections with different threshold values, the eroded design is subtracted from the intermediate design. The thickness of the enclosure can be controlled by the radius of the second smoothing filter. Step 4: the jettable enclosure is added to the smoothed design from Step 1. This can for example be done with a field summation and applying a smooth maximum with a value of 1. Also, it can help to set a void constraint on the boundary of the domain, to prevent the enclosure from adhering to the boundary.

3. Numerical examples

In this section, the numerical examples are presented and results are shown. Section 3.1 presents the optimization formulation, the two extra procedures that improve convergence and stability of optimization, and the used parameters. A 2D mechanical and a 2D thermal optimization problem are described in Section 3.2. In Section 3.3, an example is given of the enclosure method from Section 2.7. Two 3D mechanical problems are presented in Section 3.4.

3.1. Optimization formulation

For the numerical examples, two optimization problems are considered: a mechanical and a thermal compliance problem, both with a volume constraint. The design variables are the blueprint design field $\mathbf{x}$, and the final filtered design field is denoted by $\bar{\mathbf{x}}$:

$$ \begin{aligned} \underset{\mathbf{x}}{\text{minimize}}: \quad & C(\bar{\mathbf{x}}) = \mathbf{u}^T \mathbf{K}(\bar{\mathbf{x}})\mathbf{u} \\ \text{subject to}: \quad & \mathbf{K}(\bar{\mathbf{x}})\mathbf{u} - \mathbf{f} = \mathbf{0} \\ & \frac{V(\bar{\mathbf{x}})}{V^*} - 1 \le 0 \\ & 0 \le x_e \le 1 \quad \text{for} \quad e = 1 \ldots N_{\text{el}}. \end{aligned} \tag{13} $$

In here $\mathbf{K}$, $\mathbf{u}$ and $\mathbf{f}$ denote the finite element system stiffness (/conductivity) matrix, displacement (/temperature) vector and mechanical (/thermal) load vector, for the mechanical and thermal problem respectively. The objective is compliance C, the current design volume is V, the maximum allowed volume is V^*, and the number of elements in the domain is N_{el}.

The proposed filter steps described in Section 2 can sometimes suffer from undesirable convergence behavior, because the sensitivities are most pronounced at the edge of the structure. Due to this, the optimization behaves more like shape optimization rather than topology optimization. If a volume constraint is used, material is removed with high priority, until the volume constraint is satisfied, which increases the chances of ending up in an inferior local optimum. In our approach, the convergence is improved by gradually activating the jetting filter, similar to van de Ven et al. [19]. This is done by mixing the density filtered design and the jettable design:

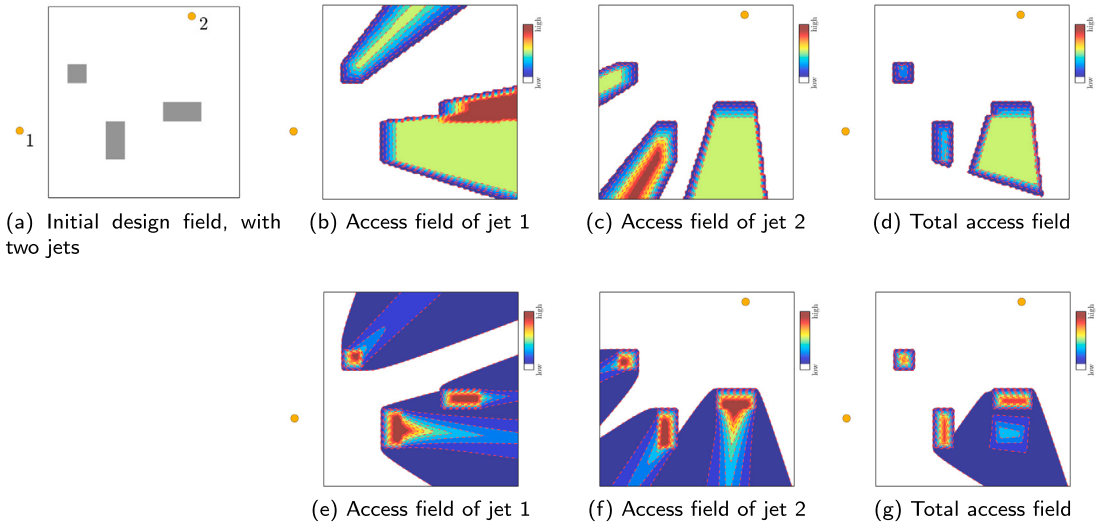

Fig. 7. Graphical representation of the combining of separate access fields into a total access field. For (b) and (c) the jet trajectory method is used, for (e) and (f) the front propagation is used. In (d) and (g), the smooth minimum fields are shown.

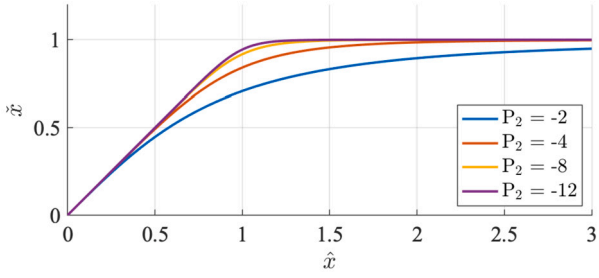

Fig. 8. The relation between the access field $\hat{x}$ and the jet access density field $\check{x}$, for different negative values of P_2.

$$\bar{x}_e(x) = (1-\eta)\tilde{x}_e + \eta\check{x}_e, \tag{14}$$

where $\eta \in [0,1]$ is the scaling parameter. In this paper η is continuously increased from 0 to 1 in the first 25 optimization iterations.

To promote numerical stability, designs should not be defined only by a blueprint density field consisting only of an outer contour, as a small change in boundary density value then can result in a large change in the overall design. To prevent boundary-only layouts, we propose to use the jet-filtered design for the volume evaluation, while the smoothed blueprint design is used for the finite element analysis. This encourages the design variables on the inside to increase, as this does hardly influence the volume, but it does increase physical performance. Note that this approach may be less effective for problems where the objective is not monotonically varying with the design variables, but this falls outside the scope of this study.

For the mapping in each element e between the smoothed density and the Young's modulus in $\mathbf{K}$ in Equation (13) the modified SIMP interpolation scheme proposed by Sigmund [17] is used, i.e.:

$$E(\tilde{x}_e) = E_{\min} + \tilde{x}_e^p(E_{\max} - E_{\min}), \tag{15}$$

with penalization exponent $p = 3.0$, minimum and maximum Young's moduli $E_{\min}$ and $E_{\max}$. For the mechanical problem, $E_{\min} = 10^{-9}$, for the thermal problem $E_{\min} = 10^{-3}$, while for both problems $E_{\max} = 1$. For the finite element analysis, 4-node quadrilateral elements with bilinear shape functions in 2D, and 8-node hexahedral elements with trilinear shape functions in 3D are used.

The 2D problem is implemented as an extension to the 88 line MATLAB code by Andreassen et al. [2], supplemented with the MMA optimizer of Svanberg [18]. The 3D problem is implemented as an extension to the PETSc code by Aage et al. [1]. The optimization is terminated after 250 iterations, by which desired level of convergence was always reached. The density filter radius is 1.5 element length l. The standard MMA values are used. An overview of the used parameters is given in Table 1.

Table 1
Summary of used parameter values.

Parameter	Value
Filter radius R	$1.5l$
SIMP exponent p	3.0
E_{min}	10^{-3} / 10^{-9}
E_{max}	1
Poisson's ratio ν	0.3
P_1	-2
P_2	-4
Number of iterations	250
Front Propagation minimum speed F_{min}	0.1

3.2. 2D problems

The first numerical example considers a 2D cantilever beam problem. This is a simple problem, with predictable optimization behavior. The boundary conditions can be seen in Fig. 10a, as well as the jet positions. A volume constraint of $V^* = 0.2$ is used, and the design domain is discretized by 100×100 elements. For comparison, the result of the standard optimization without the jetting filter is shown in Fig. 10b. As can be seen, there are many unjettable interior void regions present.

The results for the optimization with the jetting filter are presented in Fig. 11. As can be seen, no unjettable void regions exist, and the full outer surface area can be reached by at least one of the four jets. However, the compliance is approximately 70 to 80% higher than the reference design. The jet trajectory method and the front propagation method result in similar topologies, however the front propagation shows a more prevalent intermediate density region near the surfaces that are parallel to the jetting direction.

To test the robustness of the method, a heat conduction problem is also studied. The boundary conditions can be seen in Fig. 12a, as well as the positions of the jets. Again, the maximum allowed volume is $V^* = 0.2$, and a discretization of 100×100 elements. The reference design without jetting filter is shown in Fig. 12b. As can be seen, the design would be very hard to clean by jets in a 2D setting, with many small branches in an organic layout.

The results for the optimization with the jetting filter are presented in Fig. 13. The final designs differ significantly from the reference de-

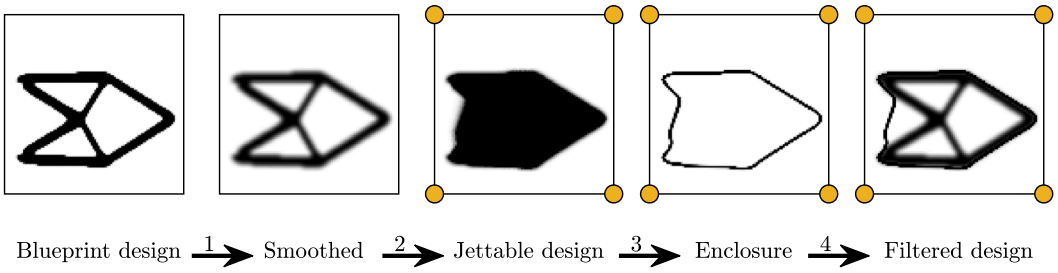

Fig. 9. Procedure to use the jet access method to only add a jettable enclosure.

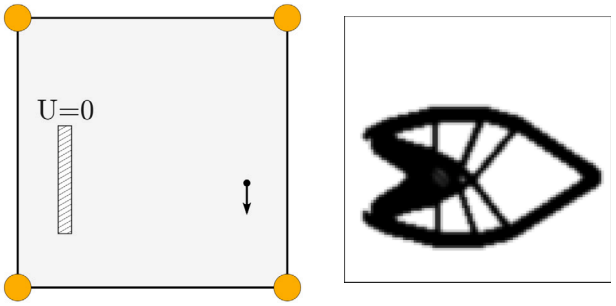

(a) Problem loading.

(b) Reference design $C := C_{\text{ref}}$

Fig. 10. The 2D cantilever beam compliance problem. In (a) the load and boundary conditions are shown with the 4 jet positions in orange. The load is applied 5% from the right edge, and 40% from the bottom. The fully clamped region is located 10% from the left edge, 40% from the bottom, and has a width of 2% and a height of 30%. In (b) the optimization result without jetting filter is shown.

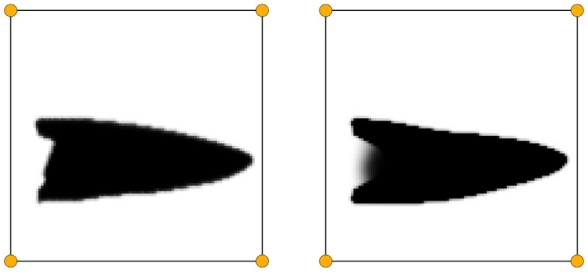

(a) Jet trajectory method. $C = 1.696C_{\text{ref}}$

(b) Front propagation method. $C = 1.817C_{\text{ref}}$

Fig. 11. The jet-filtered results of the 2D cantilever beam compliance problem, obtained with (a) the jet trajectory method and (b) the front propagation method.

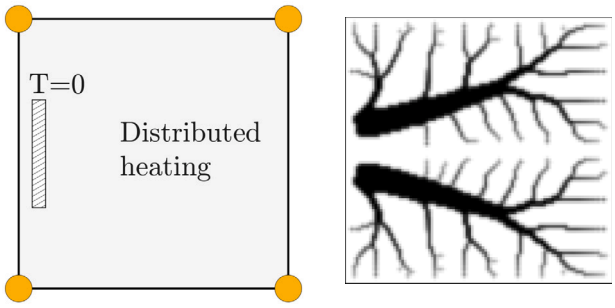

(a) Problem loading.

(b) Reference design $C := C_{\text{ref}}$

Fig. 12. The 2D heat conduction problem. In (a) the load and boundary conditions are shown with the 4 jet positions in orange. The heat sink region is located 2.5% from the left edge, 50% from the bottom, and has a width of 5% and a height of 20%. In (b) the optimization result without jetting filter is shown.

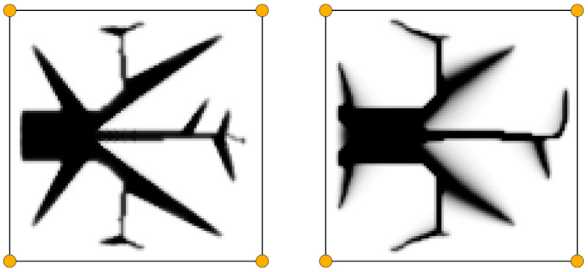

(a) Jet trajectory method. $C = 2.916C_{\text{ref}}$

(b) Front propagation method. $C = 3.985C_{\text{ref}}$

Fig. 13. The jet-filtered results of the 2D heat conduction problem, obtained with (a) the jet trajectory method and (b) the front propagation method.

sign, and are indeed jettable. However a price is paid in the objective values, which increase a factor 2.916 respectively 3.985 compared to the reference design. The designs become unsymmetrical during the optimization process for numerical reasons, no symmetry was enforced on the design. All branches are aimed at one of the jets, so their sides can still be cleaned. Also the difference in performance between the two methods is more clearly visible. Where the jet trajectory method produces clear outlines, the front propagation method has a final design with more prevalent grey regions.

Based on the numerical examples above, the performance of the two methods can be evaluated. Firstly, the jet trajectory method is strict in handling encountered solid elements, as the method computes the cumulative sum of element densities. Also the selection of targeted elements is strict, because of the Bresenham line method. Component boundaries which are in line with the jetting direction are clearly defined. On the other hand, the front propagation can be less strict with encountered solid elements, as there is a nonzero minimum speed in solid densities. Also, void regions next to the wake of solids can turn grey, because of discretization effects. These two side effects decrease the strictness, but can help with convergence. For both test problems, better objective values were obtained for jettable designs generated with the trajectory method.

Because a clearly defined boundary is preferred, we will continue this section with the jet trajectory method. For a visual validation of the performance of the method, Fig. 14 was created to show the accessibility of the boundary for each jet. The void elements are colored based on the jet they are considered reachable by. Extra lines are drawn to indicate that the long branches of the structure are parallel to a jetting direction, so that the whole surface is in fact jet accessible. However it should also be noted that these 'parallel surfaces' are on a discretized mesh, which is why some elements on the boundary of the structure seem inaccessible. This is all within a range of one element length, and is caused by the discretization.

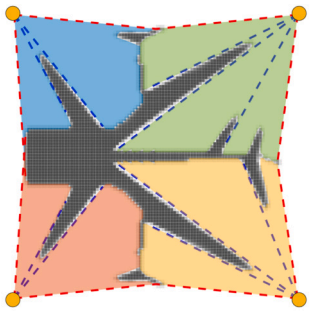

Fig. 14. Visual representation of what area can be reached by each jet, with the design from Fig. 13a.

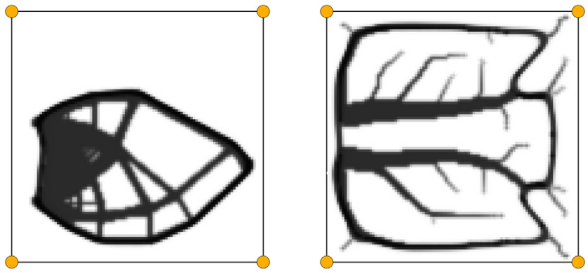

(a) Test 1. $C = 1.277C_{\text{ref}}$, with C_{ref} taken from Figure 10b

(b) Test 2. $C = 1.319C_{\text{ref}}$, with C_{ref} taken from Figure 12b

Fig. 15. The results of the 2D problems, with the jet trajectory method and the enclosure method.

3.3. 2D enclosure problem

The suggested modification of the presented filter that can create a jettable structure with internal voids, described in Section 2.7, was also tested on both 2D problems. The implementation of filter steps to create the density field $\tilde{\mathbf{x}}$ is performed as described in Section 3.1. For the creation of the enclosure field, a density filter with a radius of 8 elements is used, a Heaviside with $\beta = 7$ and $\eta = 0.5$ for the normal field, and a Heaviside with $\beta = 7$ and $\eta = 0.6$ for the eroded field. The final filtered design is obtained by taking an element-wise P-norm smooth minimum with value 1 and the element-wise sum of the smoothed field and the enclosure field, with P-norm parameter $p = -4$. As suggested, a void constraint is used on the boundary of the domain. The results can be seen in Fig. 15.

As can be seen, the final designs have a jettable enclosure as well as internal voids. Because the designs are less restricted by the filter procedure compared to not allowing internal voids, the impact on the objective value is also smaller, and for these two tests this increased approximately 30% compared to the reference design. For the simple beam problem where the reference design is already nearly jettable, all the extra filter steps in the enclosure procedure make the optimization process unnecessary complex and nonlinear. For the more complex heat problem this solution would be harder to find by an engineer. Note that in both cases the structural/thermal contribution of the enclosure is included in the optimization problem, in contrast to adding an enclosure as a post-processing step.

3.4. 3D mechanical problems

For the 3D problems, we focus on the jet trajectory method as this was found to perform best in the 2D tests. To investigate its effectiveness in a 3D setting, two tests are performed. The first example considers a simple cantilever beam. The boundary conditions can be seen in Fig. 16a, as well as the positions of the jets. A volume constraint of $V^* = 0.10$ is used, and a discretization of $144 \times 192 \times 96$ elements. For comparison, the result of the optimization without the jetting filter is shown in Fig. 16b. As can be seen, the reference design without jetting filter creates a flat cantilever beam. Since all four available jets are located at the bottom of the domain, the top of the cantilever beam would not be accessible by any of the jets. In the result with the jetting filter, visible in Fig. 16c and 16d, an additional structure is created on top of the cantilever beam. This ensures that the new top of the structure is now accessible by at least one jet. Even though the added structure contributes marginally to reduce the compliance, this part is still added to comply with the jetting requirements. In spite of the visually large design change, adding the jetting requirement comes at a cost of 38% for the objective.

The accessibility evaluation in Figs. 16e and 16f are created by taking the 0.5 density as a threshold value as solid. This design is subsequently expanded with 1 element in all directions. For all the elements in this shell it is checked if these can be reached in a straight line from any jet. These lines can go through the shell but cannot intersect the original structure. This shell is needed because when the structure is represented in a discretized manner it is possible that even accessible boundary elements are not accessible. A shell with a thickness of one element length shows the accessibility without the discretization effect. It can be seen that the reference design contains a large red surface that is not accessible by jets. The design with jetting filter in 16f on the other hand is fully jet accessible.

The second 3D example considers the MBB problem. The boundary conditions can be seen in Fig. 17a, as well as the positions of the jets. A thin local volume constraint is added to the top of the domain. The jetting filter can add material to the blueprint design up till the boundary of the domain, but for the filter its not problematic if a solid boundary is not accessible. Adding a local volume constraint gives sensitivity information for the top of the domain. A volume constraint of $V^* = 0.25$ of the relevant domain is used, and a discretization of $64 \times 192 \times 72$ elements. For comparison, the result of the optimization without the jetting filter is shown in Fig. 17b and 17c. Big parts of inside of the structure cannot be reached by any jet.

The resulting structure optimized with the jetting filter is visible in Figs. 17d-f. This design does comply with the jetting requirements. The two walls in the reference design are combined in one wall in the middle of the domain. In the previous 3D test case a feature was added on top of the structure to make all surfaces accessible, in this test case the main structure is lowered compared to the reference design, so that the jets can still reach the highest surfaces. As a result, the compliance increased by 39%. Again, an accessibility evaluation is visible in Figs. 17g and 17h.

4. Discussion

While effective, the proposed method does have several limitations. First, several assumptions are made on the jet, which can differ from specific industrial situations. In the proposed method the jet is stationary. This is a conservative assumption, since there may be cleaning scenario's where jets can be repositioned and moved. In future work we will investigate ways to take this into account. Another assumption on the jet is that it can aim in any direction. It is however quite easy to restrict this, by only consider a subset of the current jet trajectory lines. Secondly, several assumptions are made on the spray of the jet. The distance between the jet and the surface is considered irrelevant. Effectiveness of cleaning may however depend on the relative distance and angle between jet and surface, but this is not considered. Also the deflection of a jet on the surface and any secondary spray is not taken into account. Finally, to make better predictions of the jet access performance of a structure in an industrial setting, one could do a full computational fluid dynamics analysis and perform physical testing.

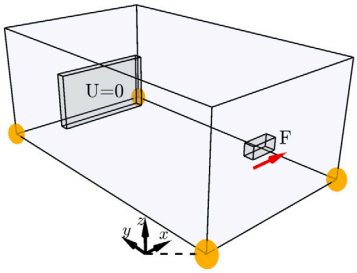

(a) Load and boundary conditions. The problem has dimensions L_x=1.5, L_y=2, and L_z=1. The load is applied in x-direction at: $x \in [0.73, 0.77]$, $y \in [0.19, 0.21]$, and $z \in [0.39, 0.41]$. The fully clamped part is located at: $x \in [0.375, 1.125]$, $y \in [1, 80, 1.90]$, and $z \in [0.2, 0.6]$. The four jets are located in all of the lower corners.

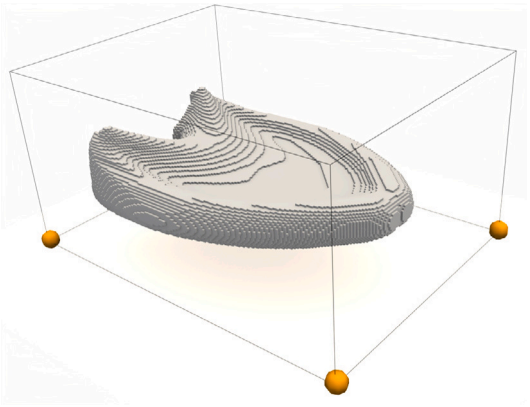

(b) Reference design without jetting filter, frontview. $C := C_{\text{ref}}$

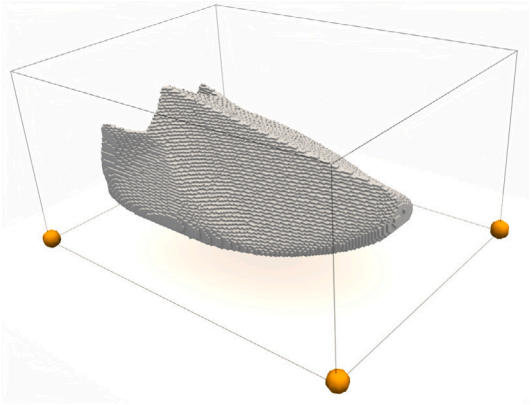

(c) Result with jetting filter, frontview. $C = 1.378C_{\text{ref}}$

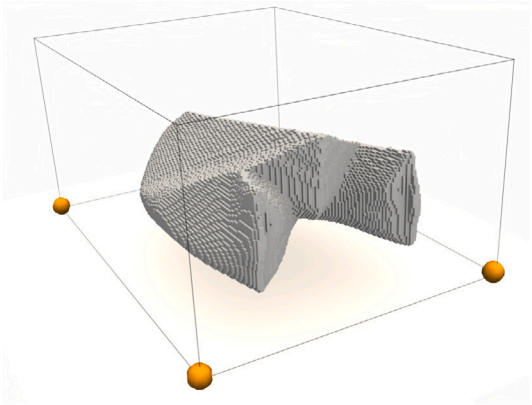

(d) Result with jetting filter, backview.

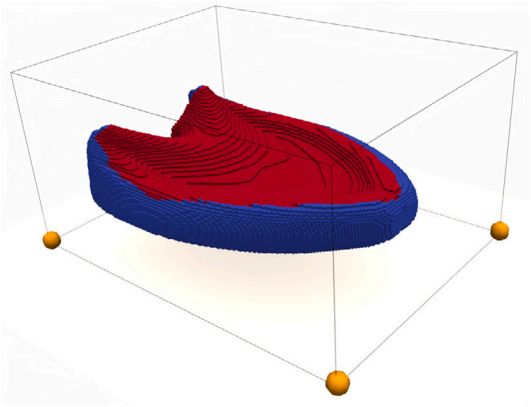

(e) Reference design, unaccessible boundary is red accessible boundary is blue.

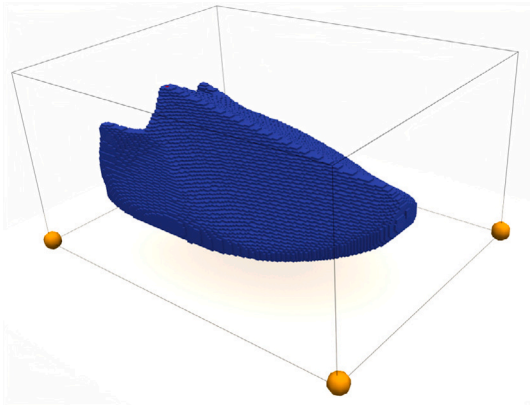

(f) Result with jetting filter, unaccessible boundary is red accessible boundary is blue.

Fig. 16. The 3D cantilever beam compliance problem optimization results, without and with the jetting filter with the jet trajectory method. Projected with a 0.5 density threshold value.

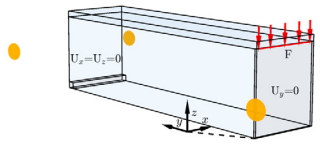

(a) Boundary conditions for the 3D bridge problem. The problem has dimensions L_x=1, L_y=3, and L_z=1.0625, where the top 0.0625 is involved in the local volume constraint. There is a symmetry boundary condition at the $x = 0$ plane, with a line load on top. The simply supported part is located at: $x \in [0, 1]$, $y \in [2.98, 3.0]$, and $z \in [0, 0.02]$. Four jets are used, located at x=-0.5|1.5, y=-0.75|3.75, and z=0.5.

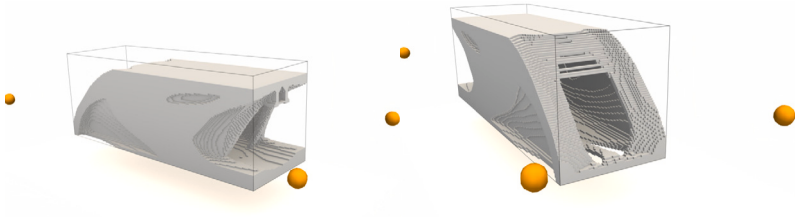

(b) Reference design without jetting filter.

(c) Reference design without jetting filter. $C := C_{\text{ref}}$

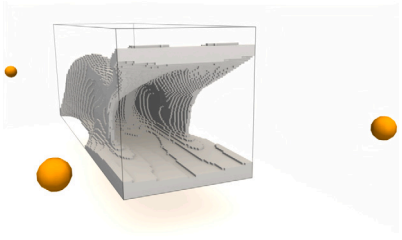

(d) Result with jetting filter.$C = 1.387C_{\text{ref}}$

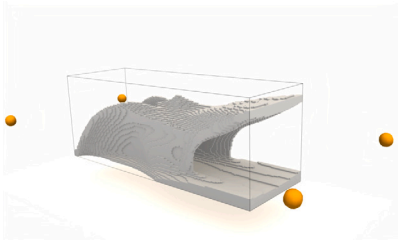

(e) Result with jetting filter.

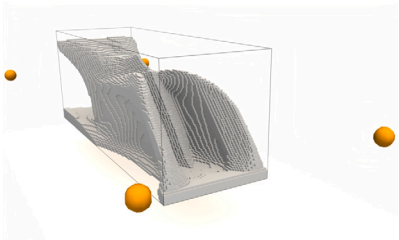

(f) Result with jetting filter.

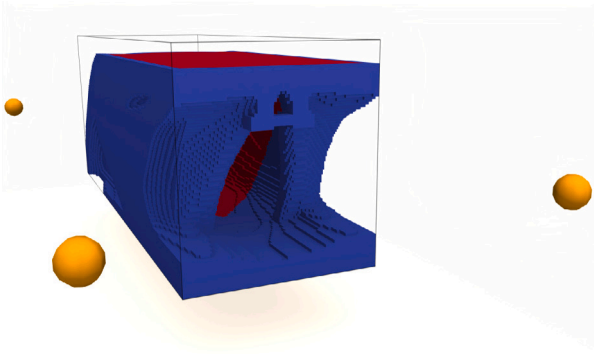

(g) Reference design, unaccessible boundary is red accessible boundary is blue.

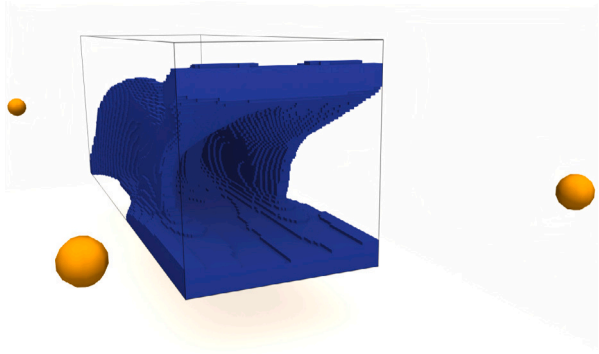

(h) Result with jetting filter, unaccessible boundary is red accessible boundary is blue.

Fig. 17. The 3D bridge compliance problem optimization results, without and with the jetting filter with the jet trajectory method. Projected with a 0.5 density threshold value.

5. Conclusion

A filter that ensures access for pressure washer jet cleaning has been proposed for density-based topology optimization. After computing an access field of each jet, these are combined into a total access field from which a jettable design field is obtained. To the best of our knowledge this is the first method to include cleanability by jetting in a topology optimization problem, and it was found to be effective in 2D and 3D numerical examples. The proposed method has several advantages. First, it is ensured that always a jettable design is obtained, because the filter turns a blueprint design into a jettable design. Because all steps are differentiable, the optimization process is performed with consistent sensitivities. Next, the method is easy to implement. The filter works as a stand alone procedure and can be used in combination with other design requirements in density based TO. Finally, no significant computational costs are added to the optimization process. This depends on several factors, such as implementation or the number of jets. For the 3D cases, with 4 jets and a non-optimized implementation, the jetting procedures increased the computation time with about 10%.

On a final note, the method does have potential to be used in other application settings. Instead of applying the filter for cleanability purposes, there is the possible usage for other applications, such as requirements for visibility and inspection, post-processing of surfaces in 3D printing, or nondestructive testing.

CRediT authorship contribution statement

Reinier Giele: Writing – original draft, Methodology. **Can Ayas:** Methodology, Writing – review & editing. **Matthijs Langelaar:** Methodology, Writing – review & editing.

Declaration of competing interest

The authors declare the following financial interests/personal relationships which may be considered as potential competing interests:

Reinier Giele reports financial support was provided by Dutch Research Council.

Data availability

No data was used for the research described in the article.

Acknowledgements

This publication is part of the project RECIPE with project number 17977 of the research programme HTSM which is (partly) financed by the Dutch Research Council (NWO). The authors wish to thank Krister Svanberg for providing the MATLAB MMA code.

References

[1] Aage N, Andreassen E, Lazarov BS. Topology optimization using PETSc: an easy-to-use, fully parallel, open source topology optimization framework. Struct Multidiscip Optim 2015;51:565–72. https://doi.org/10.1007/s00158-014-1157-0.

[2] Andreassen E, Clausen A, Schevenels M, Lazarov BS, Sigmund O. Efficient topology optimization in MATLAB using 88 lines of code. Struct Multidiscip Optim 2011;43:1–16. https://doi.org/10.1007/s00158-010-0594-7.

[3] Bourdin B. Filters in topology optimization. Int J Numer Methods Eng 2001;50:2143–58. https://doi.org/10.1002/nme.116.

[4] Bresenham JE. Algorithm for computer control of a digital plotter. IBM Syst J 1965;4:25–30. https://doi.org/10.1147/sj.41.0025.

[5] Bruns TE, Tortorelli DA. Topology optimization of non-linear elastic structures and compliant mechanisms. Comput Methods Appl Mech Eng 2001;190:3443–59. https://doi.org/10.1016/S0045-7825(00)00278-4.

[6] Campana G, Uhlmann E, Mele M, Raffaelli L, Bergmann A, Kochan J, et al. Numerical investigation into cleanability of support structures produced by powder bed fusion technology. Rapid Prototyping J 2022;28:445–52. https://doi.org/10.1108/RPJ-02-2021-0039.

[7] Chen Y, Lu J, Wei Y. Topology optimization for manufacturability based on the visibility map. Comput-Aided Des Appl 2016;13:86–94. https://doi.org/10.1080/16864360.2015.1059199.

[8] Gersborg AR, Andreasen CS. An explicit parameterization for casting constraints in gradient driven topology optimization. Struct Multidiscip Optim 2011;44:875–81. https://doi.org/10.1007/s00158-011-0632-0.

[9] Giele R, van Keulen F, Langelaar M. Design for drainability in density-based topology optimization. Struct Multidiscip Optim 2022;65:1–14. https://doi.org/10.1007/s00158-022-03272-3.

[10] Herrmann M. A domain decomposition parallelization of the fast marching method. In: Annual research briefs. Center for Turbulence Research, NASA; 2003. p. 213–25.

[11] Høghøj LC, Träff EA. An advection–diffusion based filter for machinable designs in topology optimization. Comput Methods Appl Mech Eng 2022;391:114488. https://doi.org/10.1016/j.cma.2021.114488. arXiv:2102.12999.

[12] Langelaar M. Topology optimization for multi-axis machining. Comput Methods Appl Mech Eng 2019;351:226–52. https://doi.org/10.1016/j.cma.2019.03.037.

[13] Li W, Garg S, McMains S. 2D accessibility analysis for waterjet cleaning. Comput-Aided Des Appl 2009;6:231–41. https://doi.org/10.3722/cadaps.2009.231-241.

[14] Luo Y, Li Q, Liu S. Topology optimization of shell–infill structures using an erosion-based interface identification method. Comput Methods Appl Mech Eng 2019;355:94–112. https://doi.org/10.1016/j.cma.2019.05.017.

[15] Mirzendehdel AM, Behandish M, Nelaturi S. Topology optimization with accessibility constraint for multi-axis machining. CAD Comput Aided Des 2020;122:102825. https://doi.org/10.1016/j.cad.2020.102825. arXiv:2002.07627.

[16] Sethian JA. A fast marching level set method for monotonically advancing fronts. Proc Natl Acad Sci USA 1996;93:1591–5. https://doi.org/10.1073/pnas.93.4.1591.

[17] Sigmund O. Morphology-based black and white filters for topology optimization. Struct Multidiscip Optim 2007;33:401–24. https://doi.org/10.1007/s00158-006-0087-x.

[18] Svanberg K. The method of moving asymptotes—a new method for structural optimization. Int J Numer Methods Eng 1987;24:359–73. https://doi.org/10.1002/nme.1620240207.

[19] van de Ven E, Maas R, Ayas C, Langelaar M, van Keulen F. Continuous front propagation-based overhang control for topology optimization with additive manufacturing. Struct Multidiscip Optim 2018;57:2075–91. https://doi.org/10.1007/s00158-017-1880-4.

[20] Yang J, Stern F. A highly scalable massively parallel fast marching method for the Eikonal equation. J Comput Phys 2017;332:333–62. https://doi.org/10.1016/j.jcp.2016.12.012. arXiv:1502.07303.

[21] Yoon GH, Ha SI. A new development of a shadow density filter for manufacturing constraint and its applications to multiphysics topology optimization. J Mech Des Trans ASME 2021;143:1–20. https://doi.org/10.1115/1.4048818.